

## Optimal sizing of an off-grid, renewable energy reverse osmosis desalination system based on a genetic algorithm

Daming Xu<sup>a,\*</sup>, Tom Acker<sup>b</sup>

<sup>a</sup>School of Mechanical Engineering, Xi'an University of Science and Technology, 58# Yanta RD, Xi'an 710054, China, Tel. +86 13928729859; email: xu\_daming@hotmail.com

<sup>b</sup>College of Engineering, Forestry and Natural Science, Northern Arizona University, P.O. Box: 15600, Flagstaff, AZ 86011, USA, Tel. +1 928-523-8363; email: tom.acker@nau.edu

Received 14 February 2019; Accepted 5 June 2019

---

### ABSTRACT

The purpose of this work was to find the optimal configuration for an off-grid, renewable energy reverse osmosis desalination (RO) system. The objective was to find the lowest levelized cost of energy (LCOE), with power reliability as the constraint. A genetic algorithm was used to solve the nonlinear integer programming problem. A site with brackish groundwater in Arizona, USA, was selected. The capacity of the RO system was 11.36 m<sup>3</sup>/d (3,000 gal/d), requiring a constant power consumption of 2.366 kW. The results showed that the optimal configuration was a hybrid photovoltaic/wind/diesel/battery system with LCOE 0.527 USD/kWh and the corresponding levelized cost of water 3.585 USD/m<sup>3</sup>, which were about half of the 7.9 USD/m<sup>3</sup> currently paid by residents in the area. Sensitivity analyses showed that: (a) the LCOE was fairly insensitive to photovoltaic panel tilt angle over a range; (b) the optimal tilt angle for the hybrid system must be found in the context of the performance of the entire system; (c) the “more hybrid” the renewable energy system, the lower the LCOE; (d) the LCOE value was monotone increasing as diesel price or discount rate increasing, respectively, and different diesel price or discount rate could bring different optimal configurations with diesel generators.

*Keywords:* Brackish water desalination; Reverse osmosis; Renewable energy; Optimal sizing; Genetic algorithm

---

### 1. Introduction

#### 1.1. Background

Access to affordable, reliable electricity and clean drinking water remain as two of the greatest challenges faced by the society. In 2015, the World Health Organization estimated that more than 840 million people worldwide lacked drinkable water, and that an additional 260 million had limited access, spending more than half an hour per day to collect water from improved sources [1]. Shannon et.al. [2] reported that 97.5% of all water resources on the earth are saline (in the oceans and saline aquifers); therefore

harnessing desalination to clean water could have a dramatic effect on addressing water scarcity. With regard to electricity, the International energy agency (IEA) reported that in 2016, the number of people lacking access to electricity exceeded one billion [3]. Geographically, the preponderance of these people live in the same developing areas of the world where water scarcity is an issue.

The IEA further reported that, since 2012, 34% of new grid connections had electricity provided by renewable energy (RE) sources, and that off-grid/mini-grid systems were implemented in 6% of the cases. They go on to project that by 2030, over 60% of new electricity access will be provided by renewable energy sources, and that off-grid

---

\* Corresponding author.

and mini-grid systems will provide about half of the new access [3]. The implication here is that as future water development occurs, it will frequently be coupled to renewable energy systems.

There are numerous technologies for desalinating water, all of which use thermal energy, electrical energy or a combination [4]. For brackish water resources that have lower total dissolved solids (TDS) ( $1,000 \text{ mg/L} < \text{TDS} < 10,000 \text{ mg/L}$ ) than seawater ( $>35,000 \text{ mg/L}$ ), electrically driven membrane technologies such as reverse osmosis (RO), nanofiltration and electrodialysis are practical, since the energy required to desalinate drops significantly with TDS level [5,6]. In the past two decades, desalination technologies have been improved and costs have been decreased. Desalination is currently growing at a significant combined annual growth rate of 7.4%, with RO as the dominant technology accounting for about 70% of installations [7]. In rural areas with brackish water where renewable energy resources exist, RO desalination is a good choice for water desalination [8–11].

With the need for rural development of both electricity and potable water resources, and with the emergence of renewable energy as cost competitive at off-grid sites and with some instances of grid extension, it is important to study renewable energy powered desalination. Several recent publications have reviewed renewable energy powered desalination, pointing out the advantages and challenges of employing renewable energy [8–15]. Gude and Nirmalakhandan [6] made the point that desalinating brackish water sources with renewable energy in rural regions represent “rational and logical approaches”. However, as Mathioulakis et al. [14] indicated that a major problem exists in the optimal economic design of renewable-energy-powered desalination plants, especially in remote or arid areas.

The artificial intelligence-based technics for optimal design of renewable energy hybrid power systems include genetic algorithm (GA), particle swarm optimization, evolutionary particle swarm optimization and ant colony optimization, etc. A genetic algorithm is a stochastic global search method based on natural selection, the process that drives biological evolution, and it does not require derivative or other auxiliary information. GA has several advantages: it can solve problems with multiple solutions, easy to understand and can easily be transferred to existing simulations and models, etc. GAs can be used to solve both constrained and unconstrained optimization problems [16,17].

The Southwest Navajo Nation (SNN) is a rural area in northeastern Arizona, USA, which has a large amount of accessible brackish groundwater with poor water quality [18]. The SNN has about 12,000 residents, who haul potable water, averaging  $0.38 \text{ m}^3$  (100 gal) per capita for household and livestock use. In transporting this water, residents drive an average of 48 km/d costing 3–10 USD per  $0.38 \text{ m}^3$  of potable water [19]. As a reference, this rate is approximately 10 times what people in Flagstaff, Arizona pay for water, 0.39 USD per  $0.38 \text{ m}^3$  [20]. Arizona is often called the ‘solar capital’ of the US, despite the state’s tremendous solar and other renewable resources, and this includes the SNN [21].

The Navajo Nation, in consultation with the U.S. Bureau of Reclamation, has made the decision to develop a desalination system powered by renewable energy at Leupp Coconino County, Arizona ( $35.4313^\circ\text{N}$ ,  $111.1123^\circ\text{W}$ ), where

brine pumped water physical condition is  $1,000 \text{ mg/L}$  of dissolved minerals.

The reference papers in Section 1.1 are listed in Table 1.

## 1.2. Objectives

A fresh water production of  $11.36 \text{ m}^3/\text{d}$  ( $3,000 \text{ gal/d}$ ) through RO was chosen. The objective was to find the optimal, least cost, configuration for a renewable energy reverse osmosis desalination (REROD) system, in which wind turbine generators (WTG), photovoltaic (PV) panels, a diesel generator (DG) and a battery bank are candidate power sources. The optimization problem can be formulated as a nonlinear integer programming and a genetic algorithm was used to solve it.

## 2. Problem formulations

### 2.1. Renewable energy reverse osmosis desalination system topology

Fig. 1 shows a schematic of the studied REROD system. The system consists of two main parts: an RE system and an RO system. In Fig. 1, the RO system is represented by the box in the lower left corner whereas the rest of the figure shows the components of the RE system. In the present study, the capacity of the RO system was a design condition, with a required output of clean water of  $11.36 \text{ m}^3/\text{d}$ . Consistent with recommended practice, the electric power consumption of the RO system was assumed to be constant [22], and the system was not permitted to be dispatched below its full output and was required to stay operating at all times, except when out of service for maintenance. Thus, the focus of this study was the optimal sizing of the RE system instead of the entire REROD system.

The RE system was built upon an alternating current (AC) bus. The voltage and frequency stability depends upon a DG or a cluster of bi-directional converters connected to a battery bank. The cluster of bi-directional converters is the central control unit, which dispatches the diesel power generation through a signal cable connection. The solar and wind power generation are connected to the AC bus via inverters, and the RO system gets its power supply from the AC bus.

Optimization of the RE system was broken into three distinct activities [23]:

- Simulation of RE system operation – for each candidate RE system, the performance of the entire system and each

Table 1  
Classification of reference papers in Section 1.1

Topics	References
Scarcity of drinkable water	[1,2]
Renewable energy in new electricity access	[3]
Desalination technology selection	[4–11]
Renewable energy in desalination	[8–15]
GA	[16,17]
Situation of clean drinking water in SNN, Arizona	[18–20]
Renewable resources in SNN, Arizona	[21]

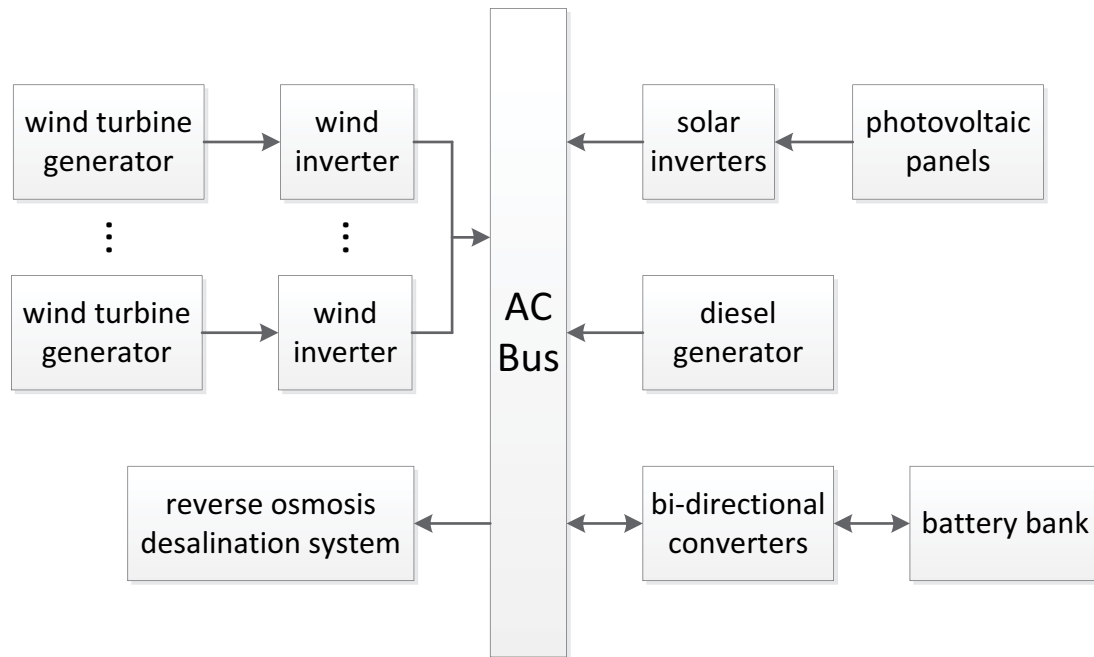


Fig. 1. Schematic of the REROD system.

of its components in serving the RO system load is simulated. In the genetic algorithm to be described later, only those RE systems that can adequately serve the system load are considered in the optimization.

- Optimization – use a genetic algorithm to select the best RE system design from the many possible alternatives based upon the objective function of minimizing the levelized cost of energy (LCOE).
- Sensitivity analysis – once an optimal design is identified, perform a sensitivity analysis to determine how sensitive the LCOE is to changes in its input parameters.

The first task undertaken to perform the optimization was to create a simulation of the RE system performance. As shown in Fig. 1, the RE system may be composed of combinations of the following components: solar PV panels, WTGs, one DG, and/or battery energy storage (batt). To perform the simulation, it was necessary to build mathematical models of each RE system component and the load, which is the RO system power consumption. In the section that follows, the RE system models will be described.

## 2.2. Models employed in the REROD system simulation

### 2.2.1. Solar energy conversion related models

#### 2.2.1.1. Hay–Davies–Klucher–Reindl model

It is necessary to compute the solar radiation incident on a tilted surface using the known radiation on a horizontal surface. The tilted surface total solar radiation consists of beam radiation and diffuse radiation from the sky and ground-reflected radiation. The diffuse radiation is the sum of three components: circumsolar and isotropic diffuse and horizon brightening. The Hay-Davies-Klucher-Reindl anisotropic model [24] was used to compute the total

hourly incident irradiance on a tilted PV panel surface,  $\bar{G}_T$ , in  $W/m^2$ :

$$\bar{G}_T = (\bar{G}_b + \bar{G}_d A_i) R_b + \bar{G}_d (1 - A_i) \left( \frac{1 - \cos(\beta)}{2} \right) \left[ 1 + f \sin^3 \left( \frac{\beta}{2} \right) \right] + \bar{G}_{pG} \left( \frac{1 - \cos(\beta)}{2} \right) \quad (1)$$

where,  $A_i = \bar{G}_b / \bar{G}_G$ , and is a function of the atmosphere transmittance regarding beam radiation.

#### 2.2.1.2. Photovoltaic panel electric power conversion model

With the total hourly incident irradiance on a tilted PV panel surface known, it is next necessary to compute PV panel average hourly output power. The computational model given by France Lasnier and Tony Gan Ang [25] was used, which defines the current–voltage relationships based on PV panel electrical characteristics. The effects of radiation level and panel temperature upon output power are considered. The output power  $P_{MP}$  from a PV panel with maximum power point tracking is given as:

$$\begin{cases} P_{MP} = V_{MP} I_{MP} \\ V_{MP} = V_{MP,ref} + \mu_{V,oc} (T_c - T_{c,ref}) \\ I_{MP} = I_{MP,ref} + I_{sc,ref} \left( \frac{\bar{G}_T}{\bar{G}_{ref}} \right) + \mu_{I,sc} (T_c - T_{c,ref}) \end{cases} \quad (2)$$

#### 2.2.2. Wind turbine generator models

Due to the high dependence of wind power on the wind speed, and because the wind speed data available was not

at the turbine hub height, the hub height wind speed was calculated using the following power-law relationship [26]:

$$V_2 = (H_2/H_1)^{\alpha} V_1 \tag{3}$$

Because the terrain is relatively flat and there is not much vegetation, a 1/7th power law boundary layer profile similar to turbulent flow over a flat plate was selected.

With an estimate of the hub height wind speed now known, the power output of a WTG can be calculated using its experimentally verified power curve. The power curve maps the power output to the hub height wind speed. The Tumo-Int series WTGs were considered in this work as typical of small turbines currently available in the market [27]. Turbines with rated power outputs of 1, 2 and 3 kW were coded a type I, II and III. Their power curves are shown in Fig. 2.

2.2.3. Diesel generator models

In order to provide continuous power to the RO system in this off-grid system, the wind and/or PV power needs to be coupled with a combustion engine, batteries or both. For this study, the combustion engine selected was a Cummins Onan QD, 5 kW, quiet commercial mobile diesel generator [28,29]. The engine’s output power-fuel curve, drawn with least-squares fitting method shown in Fig. 3, was used to calculate the diesel fuel consumption.

The filters, which are for diesel, air and lubricant, need replacement every 500 working hours [30]. The DG was set to run at 50%–75% of its rated power for fuel efficiency and mechanical health. When use of a DG was required, the RO system power consumption was about 50% of the DG rated power, thus guaranteeing a minimum DG load rate. In the simulation, the DG could be set to turn on when the battery state of charge (SOC) falls below a user-defined threshold, as will be described in a following subsection.

2.2.4. Models of lead acid batteries

Due to their long history of use and well understood cost and maintenance characteristics, lead-acid batteries were selected for this study. To calculate battery lifetime, the Ampere-hour (Ah) counting model [23] was used. The depth of discharge (DOD)-cycles to failure relations for general valve regulated lead acid (VRLA) batteries were chosen. Fig. 4 shows the VRLA battery lifetime curves [31]. The DOD is the absolute discharge relative to the rated cell capacity, which is assumed to remain unchanged as it ages [32]. For the Ah counting model, battery lifetime Ah throughput is obtained by multiplying the lifetime throughput coefficient and the rated Ah capacity. This model is employed in the commercially available renewable energy off-grid optimization software HOMER, in which there is an assumption that DOD does not affect the lifetime throughput. In the present work, the mean lifetime Ah throughput is the mean lifetime throughput coefficient multiplied by the rated Ah capacity. The battery bank lifetime is given as:

$$R_{batt} = \min \left( \frac{N_{batt} Q_{lifetime}}{Q_{thrp}}, R_{batt,f} \right) \tag{4}$$

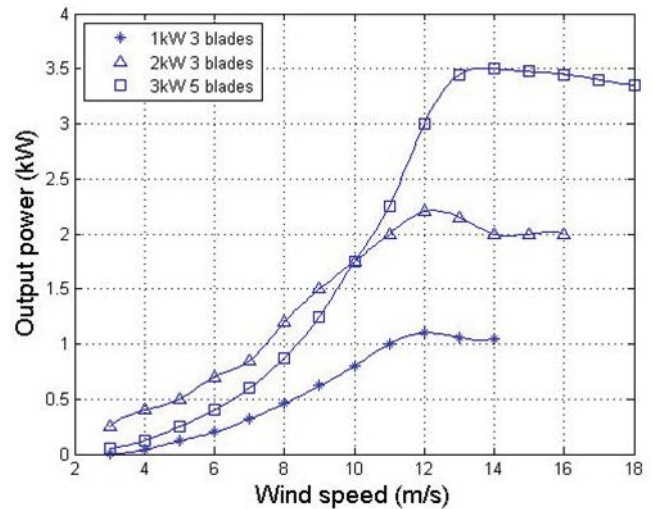


Fig. 2. Power curves for the Tumo-Int series WTGs (symbols are from the product data sheet [27]).

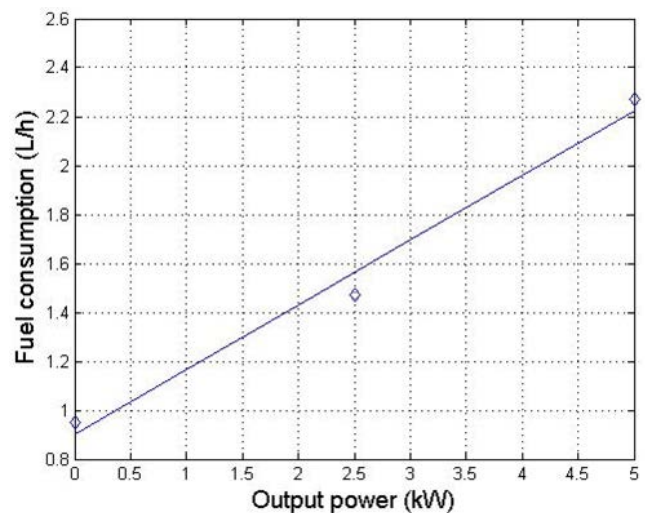


Fig. 3. Output power–fuel consumption curve of Cummins Onan Commercial QD 5 kW diesel generator (the three points are from the specification data sheet [28]).

VRLA 200Ah, 2 V batteries were used, with 24 batteries connected in one string, summing to 48 V per string. The mean lifetime throughput coefficient of the batteries was 587.5, thus the VRLA battery mean lifetime Ah throughput was 587.5 × 200 = 117,500 Ah. The batteries have a round-trip efficiency of 0.85 [33] and the DOD was set as 50% to avoid deep discharge which harms the batteries and shortens their lives.

2.2.5. Power conditioning equipment models

The solar inverters, wind inverters, and bi-directional converters were modeled using conversion efficiencies. The bi-directional converter working efficiency depends on its role as an inverter or rectifier. The specific equipment selected for use in this off-grid system will be described later.

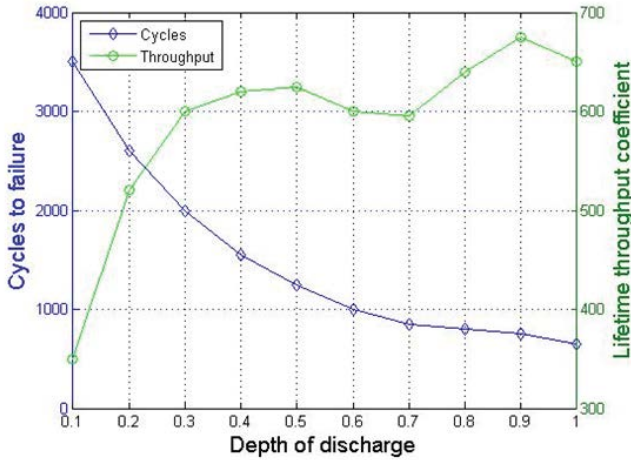


Fig. 4. Lifetime curves of a general VRLA battery (average lifetime throughput coefficient is 587.5).

### 2.2.6. Modeling of RO desalination

The electric power required for desalination  $P_{DEM}$  is affected by the hourly volumetric water demand  $H_{WD}$  of the RO system and the mean specific energy consumption for desalination  $S_{DC}$ . That is [34],

$$P_{DEM} = H_{WD} S_{DC} \quad (5)$$

The average energy consumption for RO system technology ranges from 3.7 to 8 kWh/m<sup>3</sup>, and generally the smaller the size the higher the power consumption [35]. The power consumption was set at 5 kWh/m<sup>3</sup> for the RO desalination unit, given the brackish water quality available at the site [22], and including the well pump and energy recovery devices.

Traditionally desalination systems are designed to operate with a constant power input. Usually, an unstable power input makes the desalination system operate in non-optimal conditions and this may cause severe operational problems. For example, due to power supply variation, frequent starting and stopping and partial load operation can lead to scaling, fouling, and unpredictable phenomena of membranes in RO systems [22]. The RO equipment capacity was selected as 11.36 m<sup>3</sup>/d (3,000 gal/d) according to the fresh water demand, and the RO system is assumed to work at its constant and rated electric load. Under these conditions, the  $H_{WD}$  is 0.47 m<sup>3</sup>/h and the hourly average power consumption is 2.366 kW.

In the RO system the fresh water tank volumetric capacity is proportional to the daily fresh water demand  $D_{WD}$ . To ensure desalination system autonomy, 2 d storage period was chosen [34], so the fresh water tank volume  $V_{tank}$  is

$$V_{tank} = 2D_{WD} \quad (6)$$

### 2.3. RE system operation simulation

The logistic model and time series method [36] were used for the simulation. Logistical models are employed

for long-term performance predictions and system sizing. Within each time step of the simulation, an energy balance approach is adopted where energy is conserved at each time step and throughout the entire simulation.

The simulation period was one year and the time step was one hour. During each time step, the solar, wind and diesel energy and load were assumed to be constant. The energy generated by the WTGs, PV panels and the DG for hour  $t$ ,  $E_{gen,t}$ , is expressed as:

$$E_{gen,t} = N_{WTG} E_{WTG,t} \eta_{inv,wind} + N_{PV} E_{PV,t} \eta_{inv,solar} + E_{DG,t} \quad (7)$$

If the energy generated from the PV panels, WTGs and the DG exceeds that of the RO load demand, the battery bank will be charged. Thus, if charging, at the end of hour  $t$ :

$$E_{batt,t} = E_{batt,t-1} (1 - \sigma) + (E_{gen,t} - E_{load,t}) \eta_{rect,bi} \eta_{ch,batt} \quad (8)$$

If the load demand is greater than the energy generated, then the battery bank will be discharged with the amount to cover the deficit. At the end of hour  $t$ , if discharging, the energy stored in the battery bank is given by:

$$E_{batt,t} = E_{batt,t-1} (1 - \sigma) - \frac{(E_{load,t} - E_{gen,t})}{(\eta_{disch,batt} \eta_{inv,bi})} \quad (9)$$

### 2.4. System dispatch and power reliability

In order to supply the electrical load, the power resources were dispatched in the following order [37]:

- the WTGs and PV panels
- the batteries
- the DG

The micro-cycling dispatch strategy [38] was employed. The generator starts when the battery SOC drops to a defined SOC set point ( $SOC_{start}$ ), and stops if the renewable energy production plus the battery bank can cover the load. The  $SOC_{start}$  is determined based upon a defined permissible DOD, as follows:

$$SOC_{start} = 1 - DOD \quad (10)$$

Generally, DOD = 0.5 is safe for VRLA batteries lifetime. The batteries SOC at the end of hour  $t$   $SOC_t$  is:

$$SOC_t = \frac{E_{batt,t}}{E_{batt, rated}} \quad (11)$$

Ideally, the battery bank is recharged from renewable energy as much as possible. However, if at the beginning of a time step the  $SOC_t < SOC_{start}$ , then the DGs are instructed to start and produce power for the hour. In the next time step, if renewable energy plus the battery bank covers the load and  $SOC_t > SOC_{start}$ , then the DGs stop; otherwise, the DGs keep running. When the  $SOC_t = 1$ , and if there is excess renewable energy, the renewable power generation will be constrained.

If there is not a DG in any particular configuration of the hybrid power system being simulated, then any unmet electric load demand must be recorded, and there will be no water production because the RO system shuts down. When the generated energy plus that stored in the batteries is insufficient to satisfy the load demand for hour  $t$ , that deficit is tabulated as the “loss of power supply” (LPS) for hour  $t$ , and can be expressed as:

$$LPS_t = E_{load,t} - \left( E_{gen,t} + (E_{batt,t-1} - E_{batt,rated} SOC_{start}) \eta_{disch,batt} \eta_{inv,bi} \right) \quad (12)$$

The loss of power supply probability (LPSP) over the period of the simulation,  $T$ , for example, over the course of a year, is the ratio of the sum of  $LPS_t$  values to the sum of the electric load demand throughout that period, as defined by [16]:

$$LPSP = \frac{\sum_{t=1}^T LPS_t}{\sum_{t=1}^T E_{load,t}} \quad (13)$$

The LPSP is the power reliability index of the RE system. The power reliability can be guaranteed when a DG is in the power system (assuming the fuel tank for the DG is appropriately sized), while it cannot necessarily be guaranteed in a pure renewable energy system. Because the RO system needs to work at a constant rated load and because it is desirable to run the RO continuously between its maintenance intervals (no shut downs), any power system configuration with an  $LPSP > 0$  was discarded as an infeasible solution.

### 2.5. Cost functions

The LCOE calculation method used by U.S. Department of Energy [39] was employed for the RE system,

$$LCOE = \frac{\sum_{j=1}^n \frac{I_{p,j} + M_{p,j} + F_{p,j}}{(1+r)^j}}{\sum_{j=1}^n \frac{E_j}{(1+r)^j}} \quad (14)$$

where  $I_p$ ,  $M_p$  and  $F_p$  represent the investment, maintenance and operations, and fuel costs of the RE system,  $E$  is the energy produced, and  $r$  is the discount rate. Table 2 lists the items considered in the LCOE analysis of the RE system. When equipment replacements occur, the investment expenditures are used in that year.

Following the definition of LCOE presented above, the levelized cost of water (LCOW) is defined below, which could also be employed as the cost function for the REROD system,

$$LCOW = \frac{\sum_{j=1}^n \frac{(I_{p,j} + M_{p,j} + F_{p,j}) + (I_{RO,j} + M_{RO,j}) + (I_{tank,j} + M_{tank,j})}{(1+r)^j}}{\sum_{j=1}^n \frac{Q_{W,j}}{(1+r)^j}} \quad (15)$$

Note  $Q_w$  is the quantity of water produced over the analysis period (annually in this study), and that the RO system life cycle cost, as indicated by the LCOW, is an annualized cost that takes into consideration the time value of money. It is similar to the LCOE but includes the RO system and tank capital cost and their operation and maintenance cost. The RO system operation and maintenance costs include its maintenance cost, the membrane replacement cost and chemicals costs [34].

As the capacity and electric power consumption of the RO system can be predetermined and is unchanging because the output is assumed constant (no dispatch), the optimal sizing of the RE system was studied instead of the entire REROD system. Therefore, the LCOE was adopted as the objective function in sizing the RE system. The LCOW is also an important index in terms of desalination.

### 2.6. Optimization problem formulation

The optimal sizing of the RE systems was formulated as a single criteria integer programming as:

$$\left\{ \begin{array}{l} \min \text{ LCOE} \\ \text{s.t.} \\ \text{LPSP} \leq \text{LPSP}_{set} \\ \text{Type}_{WTG} = \text{I, II, III, } \dots \\ N_{WTG} = 0, 1, 2, \dots \\ \beta = 0^\circ, 1^\circ, 2^\circ, \dots, 90^\circ \\ N_{PV,p} = 0, 1, 2, \dots \\ N_{batt,p} = 0, 1, 2, \dots \\ N_{DG} = 0, 1 \end{array} \right. \quad (16)$$

where:

$$N_{PV} = N_{PV,s} N_{PV,p}$$

$$N_{batt} = N_{batt,s} N_{batt,p}$$

The objective was to minimize the LCOE of the RE system. The LPSP was set as the constraint for feasible solutions, and is represented by the  $LPSP_{set}$ . The WTG types and sizes, PV panel tilt angles and sizes, battery capacities and DG sizes have a considerable influence on the power reliability and LCOE and can be optimized. For convenience, in every solution only one type of WTGs was applied. All the decision variables were integers. The optimization is a nonlinear integer programming problem with the constraint calculated by simulation.

From a practical point of view, the amount of radiation received using PV panels with a fixed tilt angle equal to the latitude is only slightly less than that using a monthly adjusted tilt angle. The fixed tilt angle method was employed because it would require less-expensive equipment and less maintenance [40]. The fixed tilt angle that would produce the most energy over the course of a year depends on the meteorological and topographical conditions of the location. In this optimization study, the fixed tilt angle was set

Table 2  
Items considered in LCOE analysis

	WTG	PV panel	DG	Wind inverter	Solar inverter	Bidirectional converter	Battery
$I_p$	*	*	*	*	*	*	*
$M_p$	*	*	*	*	*	*	*
$F_p$			*				

as an integer in degrees with a possible range of tilt angles from  $[0^\circ, 90^\circ]$ .

2.7. Genetic algorithm

The flowchart of the GA used in this research is shown in Fig. 5. Each block in the flowchart identifies an important step in the process, each of which are described further below. The REROD system simulation, economic computation and GA optimization codes were written in the software package MATLAB. The GA functions used were from the Complex Optimization and Decision-Making Laboratory, University of Sheffield [17].

2.7.1. Operation parameters

At the beginning of the program set the operational parameters, which include the number of individuals  $N_{ind}$ , crossover rate  $R_{cro}$ , mutation rate  $R_{mut}$ , number of generations  $N_{iter}$ , LPSP<sub>set</sub>, SOC<sub>start</sub> and lifetime of the system,  $n$ , in number of years.

2.7.2. Initializing population

Integer encoding was used and the population data structure was given as:

$$\text{Population} = \begin{bmatrix} g_{1,1} & g_{1,2} & \dots & g_{1,L_{ind}} \\ g_{2,1} & g_{2,2} & \dots & g_{2,L_{ind}} \\ \cdot & \cdot & \dots & \cdot \\ g_{N_{ind},1} & g_{N_{ind},2} & \cdot & g_{N_{ind},L_{ind}} \end{bmatrix} \quad (17)$$

Each row corresponds to an individual in the population, where an individual represents one possible configuration of the RE system. The elements in each row represent the decision variables that characterize that individual. For example,  $g_{1,2}$  represents decision variable 2 in individual 1. The decision variables of an individual are sequenced in the following order:  $[Type_{WTG}, N_{WTG}, \beta, N_{PV,p}, N_{batt,p}, N_{DG}]$ , representing the type of WTG, the number of WTGs, the tilt angle of the PV, the number of strings of PV in parallel, the number of battery strings in parallel, and the number of DGs. After a population of individuals is created, each individual is run through a simulation of its performance over 8,760 h of 1 year. The LPSP of every individual is calculated in the simulation, and inspected to see if  $LPSP > LPSP_{set}$ . The refusal strategy was used, and individuals not up to grade

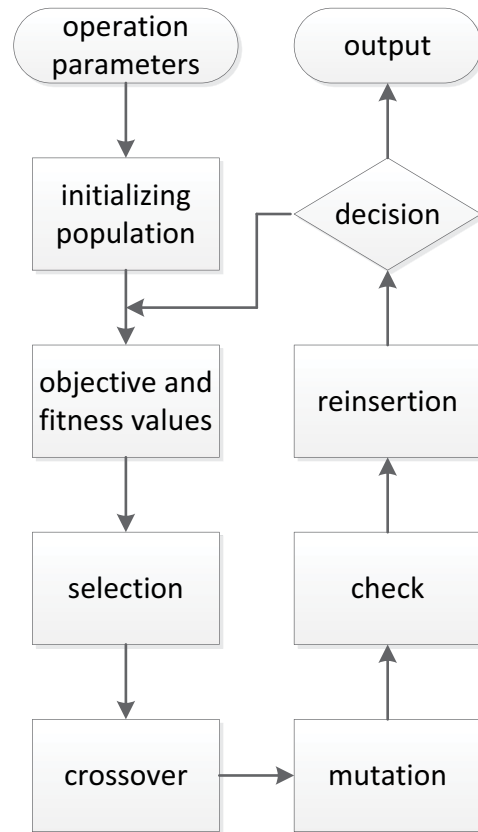


Fig. 5. Flowchart of the GA [17].

are given up and new individuals are created and checked until the whole population is formed.

2.7.3. Objective and fitness values

For individuals that meet the LPSP requirement, their objective values, LCOE, are computed. The ranking algorithm is suitable for minimization of the objective function. Individuals are marked with fitness according to their rank in the population instead of their raw performance, so local convergence can be prevented.

2.7.4. Selection

Selection is the process of determining the number of offspring that an individual will produce. Based on the fitness of individuals, a probabilistic selection of individuals is carried out. The roulette wheel selection method was employed.

### 2.7.5. Crossover

Crossover brings new individuals that have some parts of the parent's genetic information.

### 2.7.6. Mutation

Mutation provides a guarantee that the probability of searching any of the solution space will never be zero, and acts as a safety net to recover good genetic information that may be lost during the action of selection and crossover. A high mutation rate can increase the level of possible exploration of the solution space without influence on the convergence characteristics.

### 2.7.7. Check

The individuals produced from the previous steps must be checked to ensure they meet LPSP requirement. The refusal strategy was employed, and individuals not up to grade are given up and new individuals are created.

### 2.7.8. Reinsertion

To maintain the scale of the population in each generation, the child individuals are reinserted into the father population. When selecting which members of the father population should be replaced, the most common strategy is to replace the least fit members. This method can effectively implement an elitist strategy in which the most fit individuals will probabilistically survive through successive generations. With this method, a high crossover rate and mutation rate can be employed to improve the GA's performance without more stochastic fluctuations. Rudolph has proven that with an elitism strategy GAs can converge to the global optimal solution [41].

### 2.7.9. Termination decision

The GA is terminated after a pre-defined number of generations. The number of generations is chosen based upon experience. The objective function can also be plotted vs. generation to see if it has indeed come to a minimum. If it has not, the number of generations can be increased, or other parameter settings of the GA modified.

## 3. Data

The third-version typical meteorological year data sets (TMY3s) contain hourly solar radiation data and meteorological data for a 1-year period [42]. The location of Winslow, Arizona, at latitude 35.033°N and longitude 110.717°W, and elevation 1,490 m was chosen, which is nearest to Leupp among the locations in TMY3s. The data of global horizontal radiation, diffuse horizontal radiation, extraterrestrial horizontal radiation, temperature and wind speed in the TMY3s were employed, with the ground reflectance as 0.2. Wind speed is assumed to be at a height of 10 m [43] above the ground surface. The global horizontal radiation and wind speed are shown in Figs. 6 and 7, respectively. Note that the radiation and wind speed are highest during

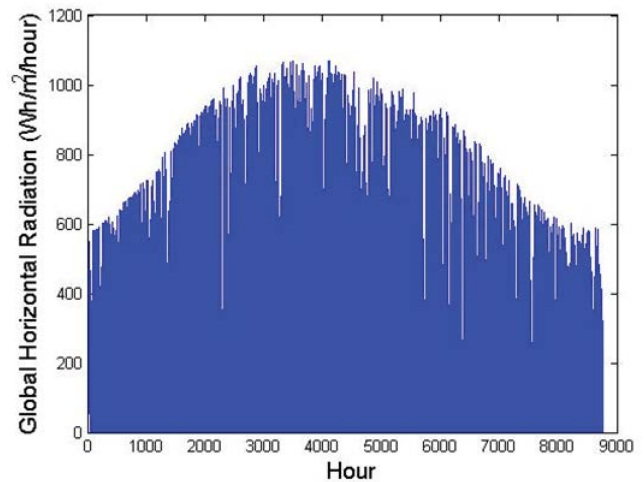


Fig. 6. TMY3 global horizontal radiation at Winslow, AZ.

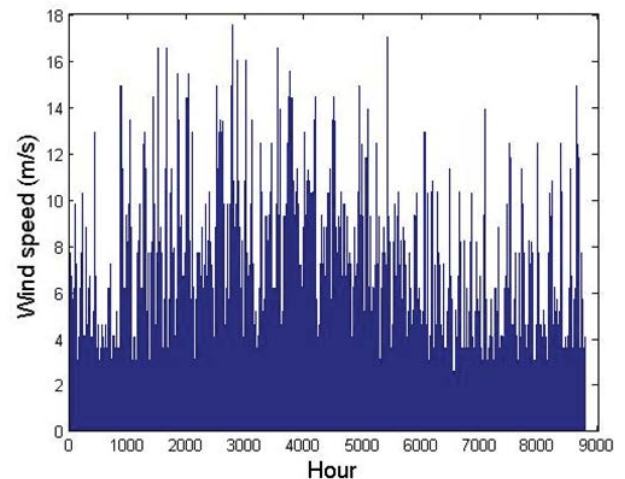


Fig. 7. TMY3 wind speed at Winslow, AZ.

the spring months, which are normally dry and windy. The radiation drops off in the summer due to seasonal monsoon rains that bring cloud cover, and the wind speed is less vigorous.

The technical specifications and economic data for each of the RE system components are shown in Table 3, along with the discount rate and project lifetime. Note that there are three types of WTGs, all from the same manufacturer. The RO and water tank specifications are taken as industry averages. The purpose of this optimization was to choose components with good, yet typical performance specifications and costs, and see what is the best configuration when faced with thousands of possible combinations of those components.

## 4. Simulation verification

Homer software [33] was used to verify the RE system simulation accuracy in this study. A configuration  $[Type_{WTG}, N_{WTG}, \beta, N_{PV,p}, N_{batt,p}, N_{DG}] = [II, 3, 35^\circ, 6, 1, 1]$  was chosen, and  $LPSP_{set} = 0$ ,  $SOC_{start} = 0.5$  and  $n = 10$  years. Parameters and

Table 3  
Technical specifications and economic data

Parameters	Value	Reference
Discount rate	3%	
Project lifetime	10 years	
<b>WTG</b> (Tumo-int)		[27]
Type and capital cost	Type I – 1 kW 3-blade, 2,000 USD Type II – 2 kW 3-blade, 4,000 USD Type III – 3 kW 5-blade, 5,000 USD	
Hub height	30 m	
Annual maintenance cost	5% of capital cost	
Lifetime	10 years	
<b>Wind inverter</b> (SMA Windy Boy)		[44,45]
Efficiency	0.93	
Capital cost	1 USD/W	
Annual maintenance cost	3% of capital cost	
Lifetime	10 years	
<b>PV panel</b> (SolarWorld SW270 Black Mono)		[46]
Maximum power	270 W	
Maximum power point current at ROCs <sup>a</sup>	8.81 A	
Short circuit current at ROCs	9.44 A	
Maximum power point voltage at ROCs	30.9 V	
Temperature coefficient for short circuit current	0.0004 A/°C	
Temperature coefficient for open circuit voltage	–0.0031 V/°C	
Module efficiency	16.10%	
Capital cost	290 USD/piece	
Annual maintenance cost	3% of capital cost	
Lifetime	20 years	
<b>Solar inverter</b> (SMA Sunny Boy)		[47,48]
Module efficiency	95%	
Capital cost	0.37 USD/W	
Annual maintenance cost	3% of capital cost	
Lifetime	10 years	
<b>DG</b> (Cummins Onan QD 5kW)		[28–30,33,49,50]
Rated power	5 kW	
Capital cost	8,135 USD	
Filters duration time	500 h	
Filters cost	50 USD	
Lifetime	10,000 h	
Cost of diesel	0.86 USD/L	
Annual maintenance cost	5% of capital cost	
<b>VRLA battery</b> (Energys PowerSafe OPzV)		[33,51,52]
Rated capacity	200 Ah, 2 V	
Charging efficiency	0.85	
Discharging efficiency	1	
Capital cost	300 USD/kWh	
Annual maintenance cost	3% of capital cost	
Lifetime	(shown in Fig. 2)	
<b>Bi-directional converter</b> (SMA Sunny Island)		[53,54]
Inverter efficiency	94.5%	
Rectifier efficiency	98%	
Capital cost	0.7 USD/W	

(Continued)

Table 3 Continued

Parameters	Value	Reference
Annual maintenance cost	3% of capital cost	
Lifetime	10 years	
<b>RO equipment</b> (Water business: DS-2)		[34,55]
Rated capacity	3,000–3,600 gal/d	
Capital cost	13,425 USD	
Maintenance cost of RO system	0.2 USD/m <sup>3</sup>	
Membrane replacement cost	0.06 USD/m <sup>3</sup>	
Number of membrane replacements per year	2	
Cost of chemicals	0.06 USD/m <sup>3</sup>	
Lifetime	10 years	
<b>Water tank</b>		[34]
Capital cost	255 USD/m <sup>3</sup>	
Annual maintenance cost	3% of capital cost	

\*ROC: reference operating condition.

Table 4  
Simulation accuracy comparison

	Homer	Simulation program	Deviation from Homer (%)
PV (kWh/year)	10,582	10,306	-2.6
WTG (kWh/year)	12,001	11,124	-7.3
DG (kWh/year)	7,974	7,995	+0.3
DG operation hour (h/year)	2,130	2,132	+0.1
Diesel consumption (L/year)	3,941	4,037	+2.4
Battery Ah throughput (kWh/year)	4,486	4,415	-1.6

<sup>a</sup>PV and wind energy generated was measured on the AC bus.

data used in the simulation program of this study were input into the Homer. The simulation accuracy comparison is shown in Table 4. The simulation results of this study are close to that of Homer. When an RE system configuration is fixed, its operational cost is mainly affected by DG operation time, diesel consumption and battery replacement (Ah throughput), etc., so the overall accuracy of the simulation program is good.

## 5. Results and discussion

The numbers of PV panels and batteries in series were determined as three and 24, respectively, in order to match the input voltage requirements of their respective inverters. The decision variables that define each individual are organized in the following order: [Type<sub>WTG</sub> N<sub>WTG</sub> β N<sub>PV,p</sub> N<sub>batt,p</sub> N<sub>DC</sub>], where β is allowed to be an integer value in the range [0°, 90°]. The simulation results for each individual includes the annual fuel consumption, DG running time and battery bank Ah throughput. These outputs were used in the LCOE cost calculation, Eq. (14). Let N<sub>ind</sub> = 500, R<sub>cro</sub> = 0.75, R<sub>mut</sub> = 0.7 and N<sub>iter</sub> = 1,000, LPSP<sub>set</sub> = 0, SOC<sub>start</sub> = 0.5. Let n = 10 years, since the lifetimes of the WTGs, wind inverters, solar inverters, bidirectional converters and RO equipment employed in this study are 10 years, and that of DGs

and batteries are shorter. Generally, in terms of engineering realization, for the next 10 years the best way is to redesign an REROD system using state of the art technologies based on the remained PV panels and water tank than to design an REROD system for 20 years at present time.

Running the GA resulted in the optimal solution [II 2 23° 6 1 1] having the lowest LCOE = 0.527 USD/kWh. The LCOE plotted vs. PV panel tilt angle is shown by the lower curve (open circle markers) in Fig. 8, and 23° and 25° bring the lowest cost. Also observe in Fig. 8 that the LCOE changes very little for tilt angles between 10° and 40°. Another interesting observation from Fig. 8 is the big jump in LCOE that occurs at a tilt angle of 73°. At this tilt angle, an additional replacement of the batteries is required causing an increase in the costs and consequently step change in the LCOE. Another typical solution [II 6 β 3 1 1] is shown as a reference in Fig. 8. For the optimal solution, as described previously, when the DG was started, it was set to run at 75% of its rated power, 3.75 kW. After powering the RO load at 2.366 kW, the remaining 1.384 kW could be utilized to charge the battery bank. The charging current was about 28.27 A after rectifiers, which is 0.14 C for a battery string. A charging current less than 0.2 C is considered good [37], and therefore the DG rated power selection is proper.

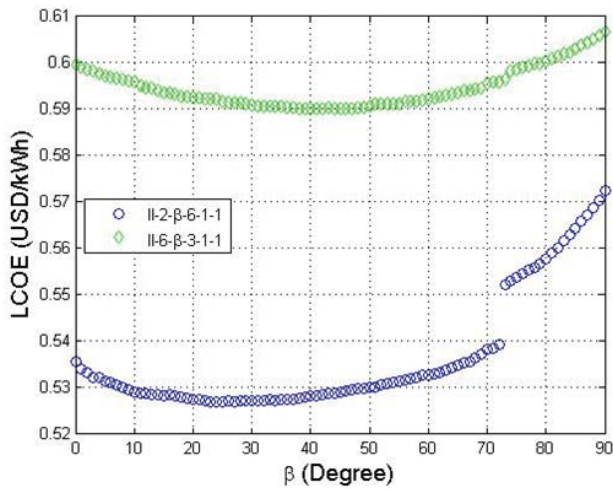


Fig. 8. LCOE vs. PV panel tilt angle for solutions [II 2  $\beta$  6 1 1] and [II 6  $\beta$  3 1 1].

For the optimal solution, the annual DG running time is 2,532 h (29% of the year), with a diesel consumption of 4,794 L, and an LCOW = 3.585 USD/m<sup>3</sup>. During the 10-year life of the system, the battery bank was changed eight times and DG four times. The LCOE of 0.527 USD/kWh is about four times of the average residential electricity price in Arizona in 2018 of 0.13 USD/kWh [56]. The LCOW of 3.585 USD/m<sup>3</sup> was more than two times the average water price in Arizona in 2017 of 1.62 USD/m<sup>3</sup> [57]. However, the LCOW is less than half of the 7.9 USD/m<sup>3</sup> currently paid by residents that live in the area, and on the lower end of the range of 3–10 USD per 0.38 m<sup>3</sup> paid for transported water by residents in the area [19].

Monthly power generation of the optimal solution is shown in Fig. 9, and the DG daily running time for 1 year is shown in Fig. 10. Both the wind and solar energy are abundant in spring and early summer, as shown in Figs. 6, 7 and 9, and the DG runs more to complement the insufficient renewable energy in the fall and winter. Monthly SOC of the battery bank is shown in Fig. 11. Note that the SOC does not fall below 0.5, and spends a majority of the time in the range of 0.60–0.85. In Figs. 9 and 11, although PV and wind energy generated in June is more than that in July, the average SOC in June is lower than that in July. The reason is the solar and wind energy is more complementary in July than that in June.

The shape of the variation of the LCOE value when plotted vs. tilt angle in Fig. 8 is consistent with and similar to shape of plots of the DG running hours and fuel consumption vs. tilt angle, both shown in Fig. 12. The same was true for the battery bank wear.

Energy outputs of the three types of WTGs for a TMY3 year is shown in Fig. 13. The type II (2 kW) WTG produces the maximum energy, which means the GA made the right choice. The optimal tilt angles of solution [II 2  $\beta$  6 1 1] were 23° and 25°, which that are less than the latitude. It is often true that a PV panel will produce the most energy over the course of a year if titled at an angle equal to the latitude, therefore it is worth considering why the optimal solution finds a different angle. Using the TMY3 data, the energy

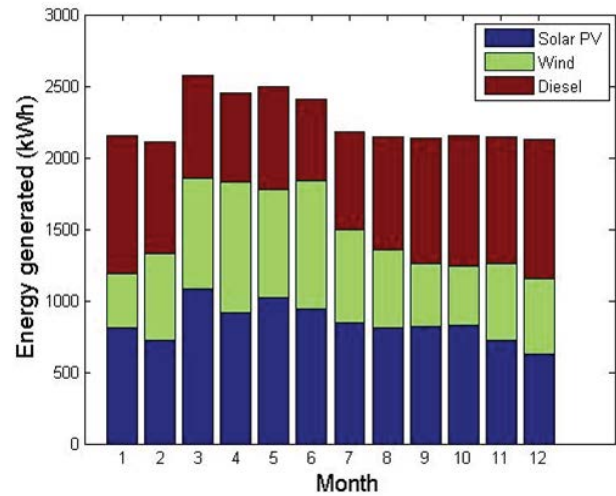


Fig. 9. Monthly power generation of the optimal solution [II 2 23° (25°) 6 1 1].

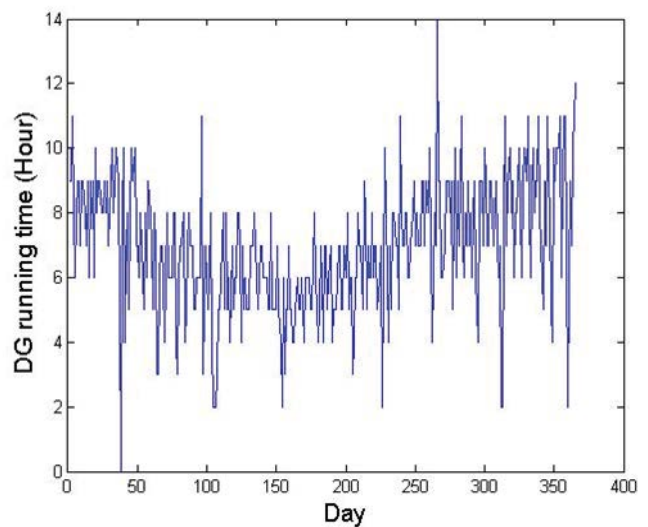


Fig. 10. DG daily running time for one year of the optimal solution [II 2 23° (25°) 6 1 1].

output of a single PV panel at this site was computed and plotted vs. tilt angle (Fig. 14), showing that the energy output is indeed the greatest when the panel tilt angle is equal to latitude. The optimal tilt angles were computed for another RE system configuration [II 6  $\beta$  3 1 1] and found to be 39°, 40° and 41°, as shown by the upper curve (open diamonds) in Fig. 8. These tilt angles are all greater than latitude. The important point here is that for a hybrid power system containing wind and solar energy, the optimal tilt angle is not necessarily equal to latitude, but rather is dependent upon the combination of energy sources and their timing. The optimal tilt angle for the hybrid system must be found in the context of the performance of the entire system and not any single component or parameter.

Fig. 15 shows a cost comparison of the optimal solutions found by the GA corresponding to the seven power system configurations a–g. The best configuration was ‘wind/PV/

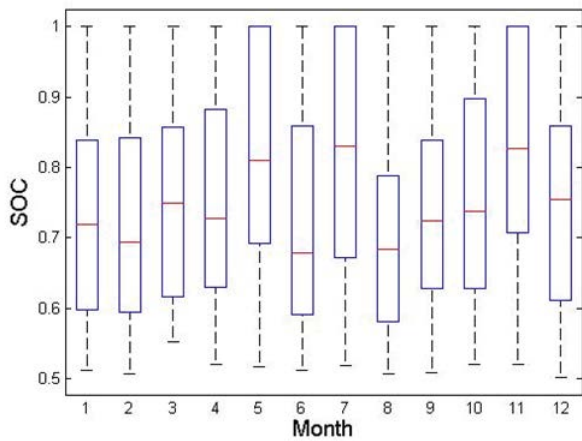


Fig. 11. Monthly SOC of the battery bank of the optimal solution [II 2 23° (25°) 6 1 1].

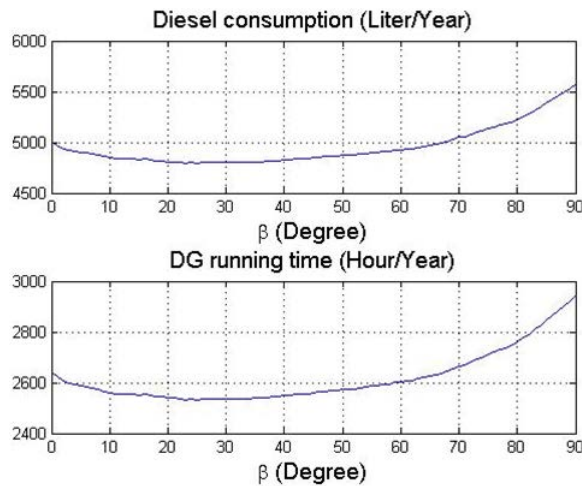


Fig. 12. Diesel consumption variation of the optimal solution [II 2 23° (25°) 6 1 1].

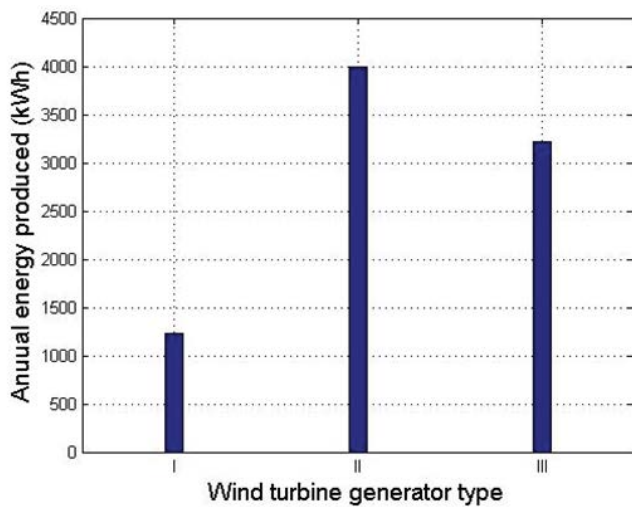


Fig. 13. Energy outputs of the three types of WTGs for a TMY3 year.

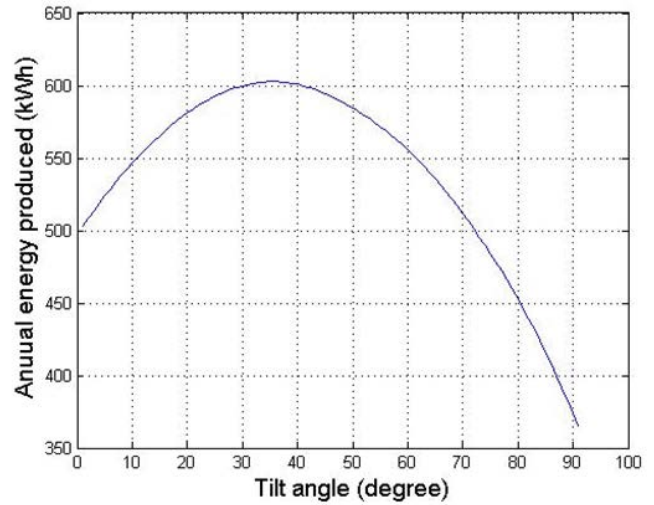


Fig. 14. One SW270 Black Mono PV panel energy output for a TMY3 year.

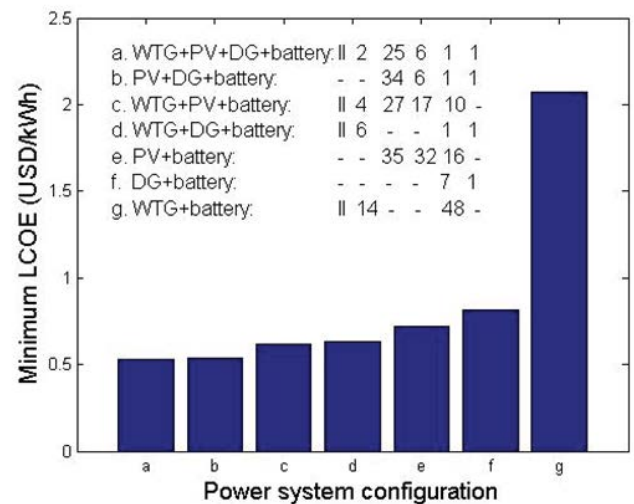


Fig. 15. Cost comparison of the optimal solutions corresponding to the seven power system configurations.

DG/battery' with its optimal solution [II 2 23° (25°) 6 1 1] and LCOE = 0.527 USD/kWh mentioned before. The next was solution [N N 34° 6 1 1] with LCOE = 0.534 USD/kWh. In considering the LCOEs for each system, notice that the costs increase when moving from left (more hybrid) to right (less hybrid). This means that hybrid systems are the most economical. The reason is that the multiple kinds of energy complement each other at this site.

The capacities of battery banks were small in the configurations that include a DG and renewable energy, while they were large in the configurations supplied only by renewable energy. Dispatchable DG can provide power at times when renewable energy is insufficient, so configurations with DGs need a small battery capacity and avoid lost energy due to the battery bank round-trip efficiency at 85%. On the contrary, configurations of pure renewable energy need dispatchable battery banks to complement the intermittent renewable energy, so the battery bank capacity is large.

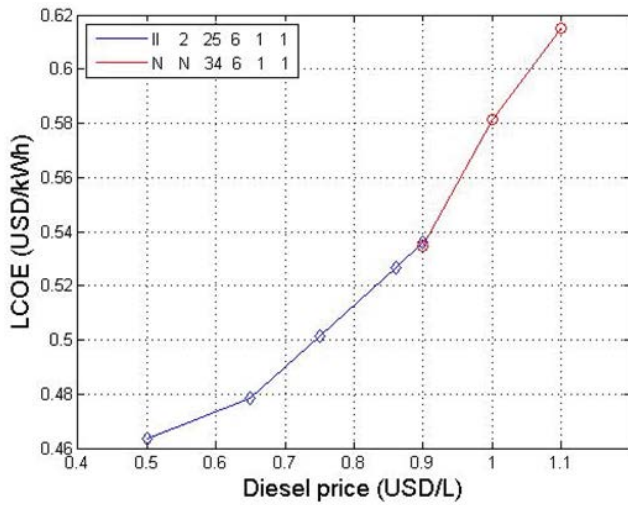


Fig. 16. Sensitive analysis on diesel price.

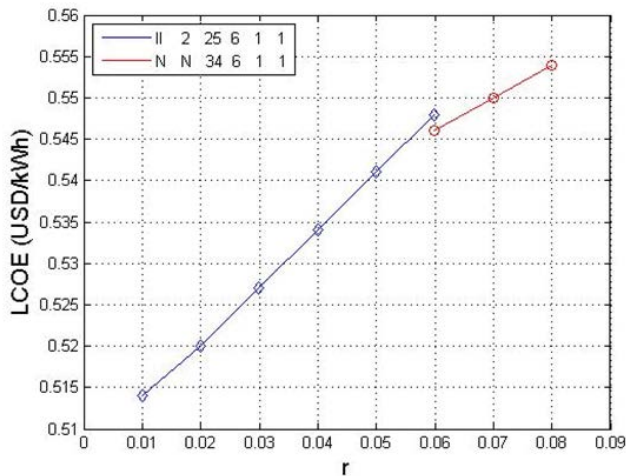


Fig. 17. Sensitive analysis on discount rate.

Fig. 16 shows the results of a sensitivity analysis on the diesel price, plotting the LCOE vs. diesel price for the optimal solutions found at each diesel price. The LCOE value was monotone increasing as diesel price increasing. In interval [0.5, 0.9] USD/L, the optimal solution was [II 2 23° (25°) 6 1 1], and in interval [0.9, 1.1] USD/L, the optimal solution was [N N 34° 6 1 1], which is the same as configuration b shown in Fig. 15. When diesel price was greater than 1.1 USD/L ‘wind/PV/battery’ won. Fig. 17 shows the results of a sensitivity analysis on the discount rate, plotting the LCOE vs. discount rate for the optimal solutions found at each discount rate. The LCOE value also was monotone increasing as discount rate increasing. In interval [0.01, 0.06], the optimal solution was [II 2 23° (25°) 6 1 1], and in interval [0.06, 0.08] the optimal solution was [N N 34° 6 1 1].

### 6. Conclusions

- The optimal configuration was [II 2 23° (25°) 6 1 1], with the lowest LCOE = 0.527 USD/kWh and the corresponding

LCOW = 3.585 USD/m<sup>3</sup>. Tilt angles 23° and 25° were optimal for this configuration. The battery bank charging current was 0.14C, which was proper, when the DG running. Sensitivity analyses showed that the LCOE was fairly insensitive to photovoltaic panel tilt angle over a range from 15° to 40°. The LCOW was less than half of the 7.9 USD/m<sup>3</sup> currently paid by residents in the area.

- For a hybrid power system containing solar energy, the optimal tilt angle was not necessarily equal to latitude. The optimal tilt angle for the hybrid system must be found in the context of the performance of the entire system and not any single component or parameter.
- The 2 kW WTG produced the maximum energy for a TMY3 year among the three types of WTGs, which meant the GA made the right choice.
- The “more hybrid” the renewable energy power system, the lower the LCOE.
- Configurations with DGs needed a small battery bank capacity, while configurations of pure renewable energy needed a large battery bank capacity.
- The LCOE value was monotone increasing as diesel price or discount rate increasing, respectively. Different diesel price or discount rate could bring different optimal configurations with DGs.

### Acknowledgements

This research was supported by the Science Research Project (No. 16JK1506) of Education Department of Shaanxi Provincial Government, P. R. China. The authors would also like to appreciate the authors of the GA toolbox in University of Sheffield for making their code freely available.

### Symbols

$A_i$	—	Index of anisotropy
$D_{WD}$	—	Daily volumetric fresh water demand, m <sup>3</sup>
$E_{batt,t}$	—	Energy stored in the battery bank at the end of hour $t$ , kWh
$E_{batt, rated}$	—	Energy stored in the battery bank when at rated capacity, kWh
$E_{DG,t}$	—	Energy generated by the diesel generator, kWh
$E_{gen,t}$	—	Energy generated for hour $t$ , kWh
$E_{load,t}$	—	Load demand for hour $t$ , kW
$E_j$	—	Electricity generation in year $j$ , kWh
$E_{PV,t}$	—	Energy generated by the photovoltaic panel, kWh
$E_{WTG,t}$	—	Energy generated by the wind turbine generator, kWh
$f$	—	Modulating factor
$F_{Dj}$	—	Fuel expenditures of the renewable energy system in year $j$ , USD
$\bar{G}$	—	Mean global horizontal irradiance, W/m <sup>2</sup>
$\bar{G}_B$	—	Direct beam part of the mean global horizontal irradiance, W/m <sup>2</sup>
$\bar{G}_D$	—	Diffuse part of the mean global horizontal irradiance, W/m <sup>2</sup>
$\bar{G}_O$	—	Average extraterrestrial irradiance at the top of the earth’s atmosphere, W/m <sup>2</sup>

$G_{\text{ref}}$	– Irradiance under reference operating conditions, $1,000 \text{ W/m}^2$	$\text{TYPE}_{\text{WTG}}$	– Type of wind turbine generators
$\bar{G}_T$	– Hourly incident irradiance on the tilted photovoltaic panel surface, $\text{W/m}^2$	$V_k$	– Wind speed at height $k$ ( $H_k$ ), $\text{m/s}$
$H_{\text{WD}}$	– Hourly volumetric water demand of the reverse osmosis system, $\text{m}^3/\text{h}$	$V_{\text{MP}}$	– Photovoltaic panel voltage at maximum power point, $\text{V}$
$H$	– Height, $\text{m}$	$V_{\text{MP,ref}}$	– $V_{\text{MP}}$ under reference operating conditions, $\text{V}$
$I_{\text{RO},j}$	– Reverse osmosis system investment expenditures in year $j$ (including financing), USD	$V_{\text{tank}}$	– Fresh water tank volumetric capacity, $\text{m}^3$
$I_{\text{MP}}$	– Maximum power point current of a photovoltaic panel, $\text{A}$	$\alpha$	– Surface roughness factor
$I_{\text{MP,ref}}$	– $I_{\text{MP}}$ under reference operating conditions, $\text{A}$	$\beta$	– Photovoltaic panel tilt angle, degree
$I_{P_j}$	– Renewable energy system investment expenditures in year $j$ (including financing), USD	$\eta_{\text{ch,batt}}$	– Battery charging efficiency
$I_{\text{SC,ref}}$	– Short circuit current under reference operating conditions, $\text{A}$	$\eta_{\text{disch,batt}}$	– Battery discharging efficiency
$I_{\text{tank},j}$	– Investment expenditures in the tank in year $j$ (including financing), USD	$\eta_{\text{inv,bi}}$	– Bidirectional converter efficiency when as an inverter
$j$	– Year $j$	$\eta_{\text{inv,solar}}$	– Efficiency of the solar inverter
$L_{\text{ind}}$	– Number of decision variables that define an individual	$\eta_{\text{inv,wind}}$	– Efficiency of the wind inverter
$\text{LPSP}_{\text{set}}$	– Loss of power supply probability set value	$\eta_{\text{rect,bi}}$	– Bidirectional converter efficiency when as a rectifier
$M_{\text{RO},j}$	– Operations and maintenance expenditures for the reverse osmosis system in year $j$ , USD	$\mu_{I,\text{sc}}$	– Short circuit current temperature coefficient, $\text{A}/^\circ\text{C}$
$M_{P_j}$	– Operations and maintenance expenditures for the renewable system in year $j$ , USD	$\mu_{V,\text{oc}}$	– Open circuit voltage temperature coefficient, $\text{V}/^\circ\text{C}$
$M_{\text{tank},j}$	– Operations and maintenance expenditures for the tank in year $j$ , USD	$\rho_G$	– Ground reflectance
$n$	– Analysis period, year	$\sigma$	– Battery hourly self-discharge rate
$N_{\text{batt}}$	– Number of batteries in the battery bank	AC	– Alternating current
$N_{\text{batt},p}$	– Number of battery strings parallel	Ah	– Ampere-hour
$N_{\text{batt},s}$	– Number of batteries in a string	DG	– Diesel generator
$N_{\text{iter}}$	– Number of generations	DOD	– Depth of discharge
$N_{\text{ind}}$	– Number of individuals in a population	GA	– Genetic algorithm
$N_{\text{PV}}$	– Number of photovoltaic panels	IEA	– International Energy Agency
$N_{\text{PV},p}$	– Number of strings of photovoltaic panels in parallel	LCOE	– Levelized cost of energy
$N_{\text{PV},s}$	– Number of photovoltaic panels in a string	LPS	– Loss of power supply
$N_{\text{WTG}}$	– Number of wind turbine generators	LPSP	– Loss of power supply probability
$P_{\text{DEM}}$	– Electric power required for desalination, $\text{kW}$	PV	– Photovoltaic
$P_{\text{MP}}$	– Photovoltaic panel maximum power point power, $\text{W}$	RE	– Renewable energy
$Q_{\text{lifetime}}$	– Battery lifetime energy throughput, $\text{Ah}$	REROD	– Renewable energy reverse osmosis desalination
$Q_{\text{thrpt}}$	– Battery bank annual energy throughput, $\text{Ah}$	RO	– Reverse osmosis
$Q_{W,j}$	– Water production in year $j$ , $\text{m}^3$	SNN	– Southwest Navajo Nation
$r$	– Discount rate	SOC	– State of charge
$R_{\text{cro}}$	– Crossover rate	TDS	– Total dissolved solids
$R_B$	– Beam radiation ratio: incident radiation on a tilted surface divided by that on a horizontal surface	USD	– United States dollar
$R_{\text{batt}}$	– Life of the battery, year	VRLA	– Valve regulated lead acid
$R_{\text{batt},f}$	– Battery float life, year	WTG	– Wind turbine generator
$R_{\text{mut}}$	– Mutation rate		
$S_{\text{DC}}$	– Average specific energy consumption for desalination, $\text{kWh/m}^3$		
$\text{SOC}_{\text{start}}$	– State of charge set point to start diesel generators		
$T_C$	– Operating temperature of the photovoltaic panel, $^\circ\text{C}$		
$T_{C,\text{ref}}$	– Photovoltaic panel temperature of $25^\circ\text{C}$ under reference operating conditions		

## References

- [1] World Health Organization, Progress on Drinking Water, Sanitation and Hygiene, World Health Organization, Geneva, United Nations Children's Fund, New York City, 2017.
- [2] M.A. Shannon, P.W. Bohn, M. Elimelech, J.G. Georgiadis, B.J. Mariñas, A.M. Mayes, Science and technology for water purification in the coming decades, *Nature*, 452 (2008) 301–310.
- [3] S. Vinci, Nigerian Electricity Regulation Commission, Ministry of Energy, R. Boampong, M.A. Phillips, C. Cader, P. Blechinger, P. Bertheau, V. Raisch, M. Moner-Girona, R. Ghanadan, M. Solano-Peralta, I. Kougiyas, K. Bódis, T. Huld, S. Szabó, S.C. Bhattacharyya, D. Palit, Energy Access Outlook 2017: From Poverty to Prosperity, International Energy Agency, Energy Procedia, 94 (2017) 144.
- [4] S. Veerpaneni, B. Long, S. Freeman, R. Bond, Reducing energy consumption in seawater desalination, *J. Am. Water Works Assn.*, 99 (2014) 95–106.
- [5] V.G. Gude, Desalination and sustainability – An appraisal and current perspective, *Water Res.*, 89 (2016) 87–106.

- [6] V.G. Gude, N. Nirmalakhandan, Sustainable desalination using solar energy, *Energy Convers. Manage.*, 51 (2010) 2245–2251.
- [7] Trends in Desalination and Water Reuse, Filtration + Separation, Available at: <https://www.filtsep.com/desalination/features/trends-in-desalination-and-water-reuse/> (accessed February 16, 2019).
- [8] M.A. Abdelkareem, M. El Haj Assad, E.T. Sayed, B. Soudan, Recent progress in the use of renewable energy sources to power water desalination plants, *Desalination*, 435 (2018) 97–113.
- [9] M. Shatat, M. Worall, S. Riffat, Opportunities for solar water desalination worldwide: review, *Sustainable Cities Soc.*, 9 (2013) 67–80.
- [10] C. Charcosset, A review of membrane processes and renewable energies for desalination, *Desalination*, 245 (2009) 214–231.
- [11] A. Al-Karaghoulis, D. Renne, L.L. Kazmerski, Solar and wind opportunities for water desalination in the Arab regions, *Renewable Sustainable Energy Rev.*, 13 (2009) 2397–2407.
- [12] V.G. Gude, Energy storage for desalination processes powered by renewable energy and waste heat sources, *Appl. Energy*, 137 (2015) 877–898.
- [13] V.G. Gude, N. Nirmalakhandan, S. Deng, Renewable and sustainable approaches for desalination, *Renewable Sustainable Energy Rev.*, 14 (2010) 2641–2654.
- [14] E. Mathioulakis, V. Belessiotis, E. Delyannis, Desalination by using alternative energy: review and state-of-the-art, *Desalination*, 203 (2007) 346–365.
- [15] S.A. Kalogirou, Seawater desalination using renewable energy sources, *Prog. Energy Combust. Sci.*, 31 (2005) 242–281.
- [16] S. Sinha, S.S. Chandel, Review of recent trends in optimization techniques for solar photovoltaic-wind based hybrid energy systems, *Renewable Sustainable Energy Rev.*, 50 (2015) 755–769.
- [17] A. Chipperfield, P. Fleming, H. Pohlheim, C. Fonseca, Genetic Algorithm Toolbox User's Guide, Version 1.2, University of Sheffield, Sheffield, Available at: [http://www.pohlheim.com/Papers/tr\\_gatbx12/ChipperfieldFlemingPohlheimFonseca\\_tr\\_GATbx\\_v12.pdf](http://www.pohlheim.com/Papers/tr_gatbx12/ChipperfieldFlemingPohlheimFonseca_tr_GATbx_v12.pdf).
- [18] J. Androwski, A.E. Springer, T.L. Acker, M.F. Manone, Wind-powered desalination: an estimate of saline groundwater in the United States, *J. Am. Water Resour. Assoc.*, 47 (2011) 93–102.
- [19] M. Haws, Solar solar desalination using distillation, USBR, Res. Dev. Off. Sci. Technol. Program, Final Rep., 2014, Proj. ID 4850, 2015.
- [20] City of Flagstaff, Water, Stormwater, and Wastewater Rates. Available at: <https://www.flagstaff.az.gov/3596/Water-Stormwater-Wastewater-Rates> (accessed January 19, 2019).
- [21] Arizona Renewable Energy Resources. Available at: [https://www.flagstaff.az.gov/DocumentCenter/View/10275/AlternativeEnergy\\_state\\_AZ?bidId=](https://www.flagstaff.az.gov/DocumentCenter/View/10275/AlternativeEnergy_state_AZ?bidId=) (accessed April 28, 2019).
- [22] V.G. Gude, Renewable Energy Powered Desalination Handbook: Applications and Thermodynamics, Butterworth-Heinemann, Oxford, United Kingdom, 2018.
- [23] F.A. Farret, M.G. Simões, Integration of Alternative Sources of Energy, IEEE Press, 2006.
- [24] J.A. Duffie, W.A. Beckman, Solar Engineering of Thermal Processes, Wiley, 2013.
- [25] F. Lasnier, T.G. Ang, Photovoltaic Engineering Handbook, Asian Institute of Technology, Bangkok, Thailand, 1990.
- [26] M.K. Deshmukh, S.S. Deshmukh, Modeling of hybrid renewable energy systems, *Renewable Sustainable Energy Rev.*, 12 (2008) 235–249.
- [27] Tumo Int Corporation Limited, Tumo-Int Wind Turbine Generators, Guangzhou, China. Available at: <http://tumo-int.com/product.php> (accessed January 20, 2019).
- [28] Commercial Generator Set Quiet Diesel TM Series QD 5000. Available at: [https://powersuite.cummins.com/PS5/PS5Content/SiteContent/en/Binary\\_Asset/pdf/Consumer/specsheets/a-1452.pdf](https://powersuite.cummins.com/PS5/PS5Content/SiteContent/en/Binary_Asset/pdf/Consumer/specsheets/a-1452.pdf) (accessed January 20, 2019).
- [29] Cummins Onan 5 HDKBC-2860 QD 5000 - 5000 Watt Quiet Diesel Commercial Mobile Generator 120 V 25 A. Available at: <https://www.electricgeneratorsdirect.com/Cummins-Onan-5-HDKBC-2860/p15742.html> (accessed January 20, 2019).
- [30] Emergency Power, 10,000 Watt Home Diesel Generator. Available at: <https://www.auroragenerators.com/products/10kw-home-diesel-generator> (accessed February 5, 2019).
- [31] R. Wust, Hybrid Power System Model How to Get the Most from your System, Inteltec 2012, IEEE, 2012, pp. 1–8.
- [32] S. Drouilhet, B.L. Johnson, A Battery Life Prediction Method for Hybrid Power Applications Preprint Work Performed Under Task Number WE712360, NREL/CP-440-21978, 1997.
- [33] HOMER - Hybrid Renewable and Distributed Generation System Design Software. Available at: <https://www.homerenergy.com/> (accessed January 20, 2019).
- [34] A. Maleki, Design and optimization of autonomous solar-wind-reverse osmosis desalination systems coupling battery and hydrogen energy storage by an improved bee algorithm, *Desalination*, 435 (2018) 221–234.
- [35] A. Al-Karaghoulis, L.L. Kazmerski, Energy consumption and water production cost of conventional and renewable-energy-powered desalination processes, *Renewable Sustainable Energy Rev.*, 24 (2013) 343–356.
- [36] J.F. Manwell, A. Rogers, G. Hayman, C.T. Avelar, J.G. McGowan, U. Abdulwahid, K. Wu, Hybrid2-A Hybrid System Simulation Model Theory Manual, National Renewable Energy Laboratory, Golden, Colorado, USA, 2006.
- [37] D. Xu, L. Kang, Optimal dispatch of unreliable electric grid-connected diesel generator-battery power systems, *Int. J. Emerging Electr. Power Syst.*, 16 (2015), doi:10.1515/ijeeps-2014-0130.
- [38] J.L. Bernal-Agustín, R. Dufo-López, Simulation and optimization of stand-alone hybrid renewable energy systems, *Renewable Sustainable Energy Rev.*, 13 (2009) 2111–2118.
- [39] DOE Office of Indian Energy, Levelized Cost of Energy (LCOE), U.S. Department of Energy, Washington, D.C., USA. Available at: <https://www.energy.gov/sites/prod/files/2017/12/f46/levelized-cost.pdf> (accessed January 7, 2019).
- [40] L.E. Hartley, J.A. Martínez-Lozano, M.P. Utrillas, F. Tena, R. Pedrós, The optimisation of the angle of inclination of a solar collector to maximise the incident solar radiation, *Renewable Energy*, 17 (1999) 291–309.
- [41] K. Deb, Multi-Objective Optimization Using Evolutionary Algorithms, John Wiley & Sons, Hoboken, New Jersey, USA, 2001.
- [42] S. Wilcox, W. Marion, Users Manual for TMY3 Data Sets, National Renewable Energy Laboratory, Golden, Colorado, USA, 2008.
- [43] T. Huld, E. Papietta, P. Zangheri, I.P. Pascua, Assembling Typical Meteorological Year Data Sets for Building Energy Performance Using Reanalysis and Satellite-Based Data, The European Commission's Science and Knowledge Service, Atmosphere (Basel), 2018.
- [44] Windy Boy 5000 Windy Boy 6000 Inverter for Wind Energy Power Plants Operating Instructions. Available at: [http://files.sma.de/dl/5661/WB50\\_60-11-FE4105.pdf](http://files.sma.de/dl/5661/WB50_60-11-FE4105.pdf) (accessed January 20, 2019).
- [45] SMA Windy Boy 5000-US 5KW Wind Inverter SB 5000US WB - Solaris. Available at: <https://www.solaris-shop.com/sma-windy-boy-5000-us-5kw-wind-inverter-sb-5000us-wb/> (accessed January 20, 2019).
- [46] SolarWorld SW270 Black Mono Solar Panel - Wholesale Solar. Available at: <https://www.wholesalesolar.com/1922269/solarworld/solar-panels/solarworld-sw270-black-mono-solar-panel> (accessed January 20, 2019).
- [47] Solar Inverters. Available at: <https://www.sma-america.com/products/solarinverters.html> (accessed January 20, 2019).
- [48] SMA Sunny Boy 5.0-US Inverter - Wholesale Solar. Available at: <https://www.wholesalesolar.com/2931725/sma/inverters/sma-sunny-boy-5.0-us-inverter> (accessed January 20, 2019).
- [49] Filters for Perkins Diesel Engines/Generators. Available at: <https://www.auroragenerators.com/collections/perkins-engine-filters> (accessed January 20, 2019).
- [50] Gasoline and Diesel Fuel Update - Energy Information Administration. Available at: <https://www.eia.gov/petroleum/gasdiesel/> (accessed January 20, 2019).
- [51] PowerSafe OPzV Batteries. Available at: [http://www.enersysteme.com/reserve/pdf/EN-PS-OPzV-RS-004\\_0414.pdf](http://www.enersysteme.com/reserve/pdf/EN-PS-OPzV-RS-004_0414.pdf) (accessed February 5, 2019).

- [52] J.P. O'Connor, *Off Grid Solar: A handbook for Photovoltaics with Lead-Acid or Lithium-Ion batteries*, Kindle Direct Publishing, Seattle, Washington, USA, 2016.
- [53] SUNNY ISLAND 4548-US / 6048-US. Available at: <https://www.sma-america.com/products/battery-inverters/sunny-island-4548-us-6048-us.html> (accessed January 20, 2019).
- [54] SMA Sunny Island 5048U 5KW Battery Inverter SI 5048U - Solaris. Available at: <https://www.solaris-shop.com/sma-sunny-island-5048u-5kw-battery-inverter-si-5048u/> (accessed January 20, 2019).
- [55] Water Business USA Manufacturer of Water Purification Equipment, Diamond skid price sheet. Available at: [http://www.waterbusiness.com/diamond\\_price.htm](http://www.waterbusiness.com/diamond_price.htm) (accessed January 20, 2019).
- [56] EIA - Electricity Data. Available at: <https://www.eia.gov/electricity/data.php> (accessed January 20, 2019).
- [57] S. Craig, 2017 Report on Water Pricing in Arizona, 2017. Available at: [https://www.azwifa.gov/media-releases/docs/2017/WIFA Water Rates Report press release.pdf](https://www.azwifa.gov/media-releases/docs/2017/WIFA%20Water%20Rates%20Report%20press%20release.pdf) (accessed January 20, 2019).